Design of High Performance Miniaturized Lowpass Filter Using New Approach of Modeling

Sohrab Majidifar

Department of Electrical Engineering
Kermanshah University of Technology, Kermanshah, Iran
s.majidi@kut.ac.ir

Abstract ─ In this paper a compact microstrip lowpass filter (LPF) is presented using the taper-loaded resonator. Based on a new approach, the resonator response as a function of its model component is obtained. The proposed equation between the insertion loss and LC parameters of the resonator, enable designers to calculate the proper amount of these parameters for a considered response, through the mathematical equations. The response of the final filter is improved using H-shape and spiral-shape defected ground structure. This filter is designed, fabricated and measured and as it is shown in the simulation results, the cutoff frequency is 1.53 GHz, the roll-off rate is better than 29.3 dB/GHz and the insertion loss is less than 0.1 dB from DC to 1.1 GHz.

Index Terms ─ Circuit model, defected ground structure, taper loaded resonator.

I. INTRODUCTION

Suppression of high frequency unwanted signals is one of the microstrip LPF's applications in microwave system [1-3]. These filters design in various shapes using different resonators but, in new structures, the main attempt is the improvement of the response parameters such as stopband bandwidth, selectivity and compactness. Researchers have used different methods to achieve these goals. Some articles have focused on sharpness improvement [4-6]. In [4], by combining three shunt open stubs, a compact LPF with very high selectivity is obtained. In this filter, sharp response with a roll off rate of 49 dB/GHz is achieved. A compact structure with high selectivity and wide stopband is designed in [5]. This filter is composed of two folded stepped impedance open stubs and a semi-circle ended suppressing cell. In [6], a novel Hilbert curve ring fractal DGS and its equivalent model are investigated, and by cascading three improved Hilbert curve ring DGS cells, a sharp response microstrip LPF is designed. The insertion loss of the passband is below 0.5 dB in this filter.

In [7-11], researchers have designed lowpass filters with wide stopband. A compact lowpass filter with wide stopband using novel windmill resonators is presented in [7]. At the 3 dB cutoff frequency of 1.76 GHz, the designed LPF achieves a wide stopband with overall 20 dB attenuation up to seven times the cutoff frequency. In order to design a lowpass filter with wide stopband, a novel meandered-slot resonator is presented in [8]. The 3 dB cutoff frequency of this filter is 2.2 GHz and this LPF achieves an ultra-wide stopband of 12.8 times the cutoff frequency with more than 20 dB attenuation. Novel compact and wide stopband elliptic-function resonator is proposed in [9]. Two broad stopband LPFs using one and two of the proposed resonators are designed. This resonator introduces four transmission zeros in the stopband and the positions of them can be tuned easily to get different stopband characteristics. A bandstop structure is embedded into classical stepped impedance lowpass filter in [10] to make the stopband wider. This filter has a small size. A novel complementary triangular split ring resonator (CTSRR) using DGS is introduced in [11]. In order to design a high-performance lowpass filter with a cutoff frequency of 1.80 GHz, CTSRR units are cascaded together. A LPF with wide stopband is developed in [12]. This filter is composed of two radial stub resonators that are asymmetrically connected to each other by a stepped impedance structure. This structure results in high rejection and wide stopband. A compact elliptic-function microstrip LPF using stepped impedance resonators loaded (SIRs-loaded) hairpin resonators are presented in [13]. Two LPFs using one-cell and two-cell is designed in this work. The two-cell filter has a 3 dB cutoff frequency at 2 GHz and a size of only 0.081 $\lambda g \times 0.096\ \lambda g$. A novel complementary split-ring resonators (CSRRs) DGS are proposed to design LPFs with excellent performance in terms of low ripple in the pass band, sharp selectivity and wide stop band [14].

The authors in [15-17] have focused on compactness in LPF design. Using an improved split ring resonator, a new compact miniaturized stepped impedance LPF is proposed in [15]. In [16], both symmetrically loaded resonant patches and meander transmission line are adopted to achieve wide stopband and compact size. A novel microstrip lowpass filter based on a T-shaped

Submitted On: May 21, 2015
Accepted On: November 8, 2015

resonator is proposed in [17] that presents a compact size. The physical size of this filter excluding the feeding lines, is 13.1 mm * 8.2 mm.

In this article, a taper loaded resonator is proposed to design a LPF with wide stopband and compact size. The proposed resonator is presented and studied with an LC model and then it is used to implement a high performance LPF.

II. PROPOSED RESONATOR

Figure 1 shows the layout, circuit model and EM simulation results of the proposed taper-loaded resonator. Resonator dimensions are as follows: L = 22 mm, L1 = 6 mm, L2 = 4 mm, L3 = 9.66 mm, W1 = 0.1 mm and W2 = 1.2 mm.

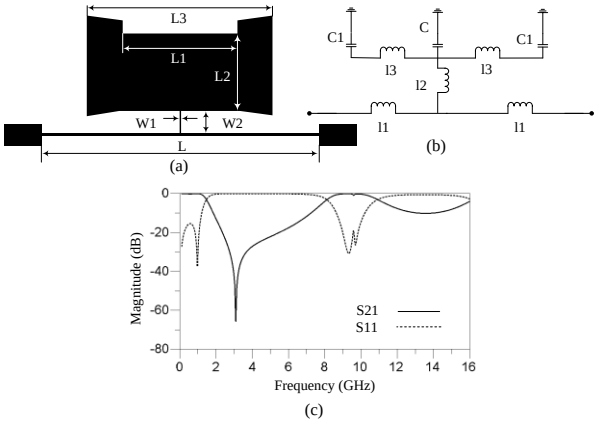

Fig. 1. Pproposed resonator: (a) layout, (b) circuit model, and (c) EM simulation results in a wide span.

As it is depicted in Fig. 1 (b), l1 introduce the inductance of the transmission line, the inductance of the high impedance stub with the length of W2 is l2, l3 shows the internal inductance of the low impedance part of the resonator and the body capacitance of the middle part and loaded tapers are presented as C and C1 respectively.

Using Equations (1-4), the LC parameters of the proposed model are calculated as follows [5], [18,19]: l1 = 7.5 nH, l2 = 1 nH, l3 = 0.3 nH, C1 = 0.55 pF and C = 1.5 pF. The calculation of the tapered parts is done using the average length of the tapers:

$$C = [8.85\ (10)^{-12}\{[\frac{\varepsilon r\ w}{h}]^{1.08} + [2\pi(\frac{\varepsilon r+1}{2})(\frac{1}{\ln(\frac{8h}{w}+1)} - \frac{w}{8h})]^{1.08}\}^{0.926}]\ l. \quad (1)$$

In the following equations, the calculated characteristic impedance (Zc) and effective permittivity (ε_{re}) are: Zc = 154 Ω and ε_{re} = 1.695 for W = 0.1 mm, Zc = 13.9 Ω and ε_{re} = 2.08 for W = 6 mm and for W = 1.83 ε_{re} = 1.94 and Zc = 36.5 Ω:

$$L = \frac{l\ z_c}{v_p}, \qquad v_p = \frac{c}{\sqrt{\varepsilon_{re}}}. \quad (2)$$

For w/h ≤ 1:

$$\varepsilon_{re} = \frac{\varepsilon_r+1}{2} + \frac{\varepsilon_r-1}{2}\{[1+12\frac{h}{w}]^{-0.5} + 0.04\ [1-\frac{w}{h}]^2\},$$
$$z_c = \frac{\eta}{2\pi\sqrt{\varepsilon_{re}}}\ln[8\frac{h}{w} + 0.25\frac{w}{h}]. \quad (3)$$

For w/h ≥ 1:

$$\varepsilon_{re} = \frac{\varepsilon_r+1}{2} + \frac{\varepsilon_r-1}{2}[1+12\frac{h}{w}]^{-0.5},$$
$$z_c = \frac{\eta}{\sqrt{\varepsilon_{re}}}\{\frac{w}{h} + 1.393 + 0.677\ln[\frac{w}{h} + 1.444]\}^{-1}, \quad (4)$$

where, C and L are capacitance and inductance of the resonator parts, v_p represents the phase velocity, w, l and h are line widths, line lengths and substrate thickness respectively, η is a constant equal to 120π Ω and c represents the light speed. The circuit and EM simulated results of the resonator are shown in Fig. 2.

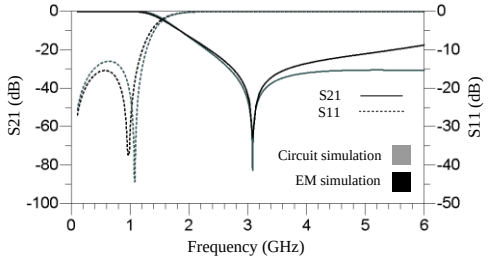

Fig. 2. EM and circuit simulation results in a narrow span.

Matching between circuit simulation and EM simulation results shows the detailed description of the proposed circuit model. Resonator response extraction as a function of the LC parameters causes that dependence of this response to each element be calculated, and using Equations (1-4) dependence of this response as a function of the resonator dimension can be calculated.

The equations where calculating the insertion loss of the resonator based on the LC parameters, are as (5-9):

$$Z_{11} = Z_{22} = 0.5\ I(+1-8\pi^2 f^2 C1\ l2 + 16\ l2\ \pi^4 f^4 C\ l3\ C1 - 4\ l2\ \pi^2 f^2 C - 4\ l3\ \pi^2 f^2 C1)\ /\ \pi\ f(-2\ C1 + 4\ l3\ C1\ \pi^2 f^2 C - C), \quad (5)$$

$$Z_{21} = Z_{12} = 0.5\ I(+1-8\pi^2 f^2 C1\ l2 + 16\ l2\ \pi^4 f^4 C\ l3\ C1 - 4\ l2\ \pi^2 f^2 C - 4\ l3\ \pi^2 f^2 C1 - 8\ l1\ \pi^2 f^2 C1 + 16\ l1\ \pi^4 f^4 C1\ l3\ C - 4\ l1\ \pi^2 f^2 C)\ /\ \pi\ f(-2\ C1 + 4\ l3\ C1\ \pi^2 f^2 C - C), \quad (6)$$

$$S_{21} = \frac{2\ Z_{21}\ Z_0}{(Z_{11}+Z_0)\ (Z_{22}+Z_0) - Z_{12}\ Z_{21}}, \quad (7)$$

$$S_{21} = (50\ \mathrm{I}(-8\ \mathrm{l2}\ \pi^2\mathrm{f}^2\mathrm{c1}+16\ \mathrm{l2}\ \pi^4\mathrm{f}^4\mathrm{C}\ \mathrm{l3}\ \mathrm{C1}-4\ \mathrm{l2}\ \pi^2\mathrm{f}^2\mathrm{C}-4\ \mathrm{l3}\ \pi^2\mathrm{f}^2\mathrm{C1}+1))\ /\ (\pi\ \mathrm{f}(-2\ \mathrm{C1}+4\ \mathrm{c}\ \mathrm{l3}\ \pi^2\mathrm{f}^2\mathrm{C1}-\mathrm{C})\ ((0.5\ I(-8\ \mathrm{l2}\ \pi^2\mathrm{f}^2\mathrm{C1}+16\ \mathrm{l2}\ \pi^4\mathrm{f}^4\mathrm{C}\ \mathrm{l3}\ \mathrm{C1}-4\ \mathrm{l2}\pi^2\mathrm{f}^2-4\ \mathrm{l3}\ \pi^2 f^2\mathrm{C1}+1-8\ \mathrm{l1}\ \pi^2\mathrm{f}^2\mathrm{C1}+16\ \mathrm{l1}\ \pi^4\mathrm{f}^4\mathrm{C}\ \mathrm{l3}\ \mathrm{C1}-4\ \mathrm{l1}\ \pi^2\mathrm{f}^2\mathrm{C})\ /\ \pi\ \mathrm{f}(-2\mathrm{C1}+4\ \mathrm{Cl3}\ \pi^2\mathrm{f}^2\mathrm{C1}-\mathrm{C})+50)^2+0.25\ (-8\ \mathrm{l2}\ \pi^2\mathrm{f}^2\mathrm{C1}+16\ \mathrm{l2}\ \pi^4\mathrm{f}^4\mathrm{C}\ \mathrm{l3}\ \mathrm{C1}-4\ \mathrm{l2}\ \pi^2\mathrm{f}^2\mathrm{C}-4\ \mathrm{l3}\ \pi^2\mathrm{f}^2\mathrm{C1}+1)^2\ /\ \pi^2\mathrm{f}^2(-2\ \mathrm{C1}+4\ \mathrm{C}\ \mathrm{l3}\ \pi^2\mathrm{f}^2\mathrm{C1}-\mathrm{C})^2)), \quad (8)$$

where "f" represents the frequency in Hz and "Z_0" is the terminal impedance. If in Equation (8), we set l1 = 7.5 nH, l2 = 1 nH, l3 = 0.3 nH, C = 1.5 pF and C1 = 0.55 pF, then S_{21} turns to a function of "f" as (9):

$$S_{21} = 50\ \mathrm{I}\ (-1.106\ 10^{-20}\pi^2 f^2+3.96\ 10^{-42}\pi^4 f^4+1)/(\pi\ \mathrm{f}\ (-2.6\ 10^{-12}+9.9\ 10^{-34}\pi^2 f^2)((0.5\ I(-8.9\ 10^{-20}\pi^2 f^2+3.366\ 10^{-41}\pi^4 f^4+1)/\pi\ f(9.9\ 10^{-34}\pi^2 f^2-2.6\ 10^{-12})+50)^2+0.25(1.1`\ 10^{-20}\pi^2 f^2+3.96\ 10^{-42}\pi^4 f^4+1)^2\ /\ \pi^2 f^2(-2.6\ 10^{-12}+9.9\ 10^{-34}\pi^2 f^2)^2)). \quad (9)$$

Figure 3 shows the magnitude of S_{21} as a function of "f" (according to the Equation (9)).

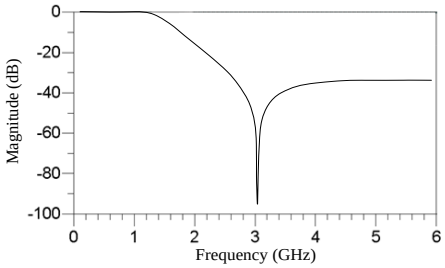

Fig. 3. Magnitude of S_{21} as a function of "f" (according to the Equation (9)).

The sharpness of the resonator is introduced by (10):

$$\Delta f = f_s - f_c, \quad (10)$$

where "f_s" is the first -20 dB point and "f_c" is the 3 dB cutoff frequency of the resonator. Let f_1 to be the smallest positive root of (11) and f_2 denotes the positive root of (12), then $\Delta f = f2 - f1$ defines the sharpness of LC resonator response:

$$A = 20\ \log|S_{21}(f)| + 3 = 0, \quad (11)$$

$$B = 20\ \log|S_{21}(f)| + 20 = 0. \quad (12)$$

Figure 4 depicts Δf in terms of l1, l2, C and C1.

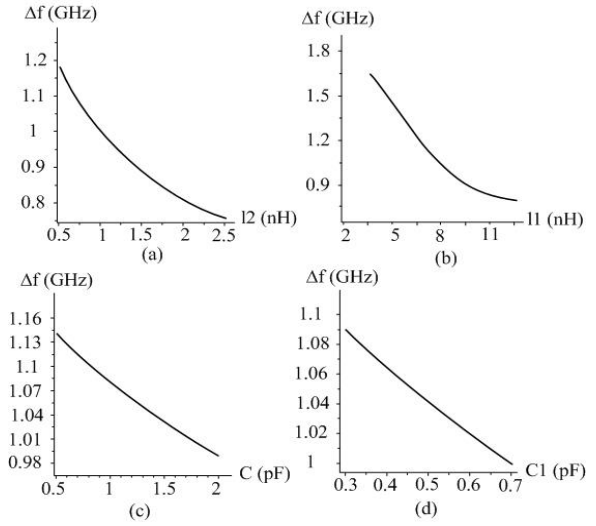

Fig. 4. Sharpness of LC resonator response as a function of l1, l2, C and C1.

III. FILTER DESIGN

As it is seen in Fig. 1 (c), the transition poles at 9.3 GHz and 9.68 GHz limit the stopband of the proposed resonator. Creating transition zeros near the pole frequencies improves the stopband bandwidth of the resonator. So, low impedance tapered stubs add to the sides of the resonator and form the basic structure of the LPF. Figures 5 (a) and 5 (b) show the layout and simulation results of the proposed resonator with added low impedance stubs.

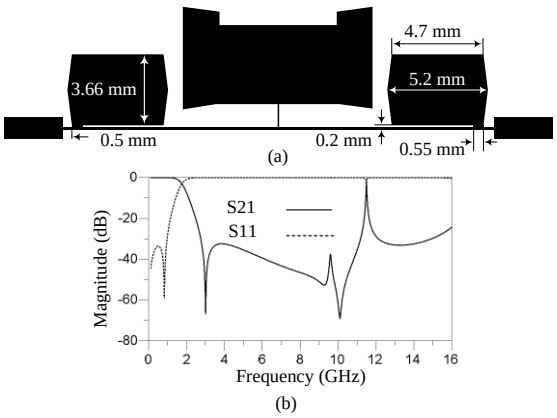

Fig. 5. Basic structure of LPF3: (a) layout and (b) simulation results.

According to Fig. 5 (b), the transition pole that is created at 11.46 GHz limits the stopband of the proposed structure. To deactivate this pole effect without size variation, the defected ground structure (DGS) is used in the final design of the LPF. The layout of the DGS spiral and H-shaped resonators are shown in Fig. 6 (a). The simulation results of the transition line with/without DGS are shown in Fig. 6 (b). As seen in this figure, a transition zero appears at 11.45 GHz when DGS is used.

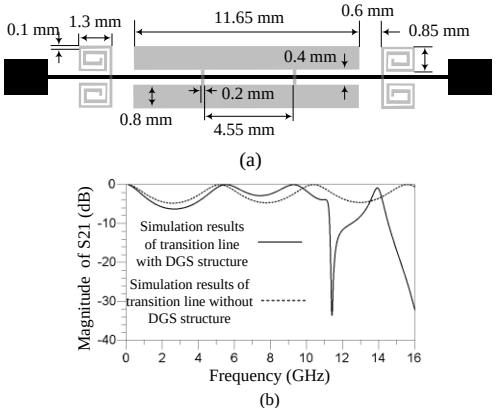

Fig. 6. Spiral and H-shaped DGS: (a) layout and (b) simulation results.

As it is shown in Fig. 6 (b), the transition zero that is created by DGS deactivates the transition pole of the basic structure (at 11.46 GHz) and expand the stopband of the filter response. Layout, fabrication picture and simulation/measurement results of the proposed LPF are presented in Fig. 7.

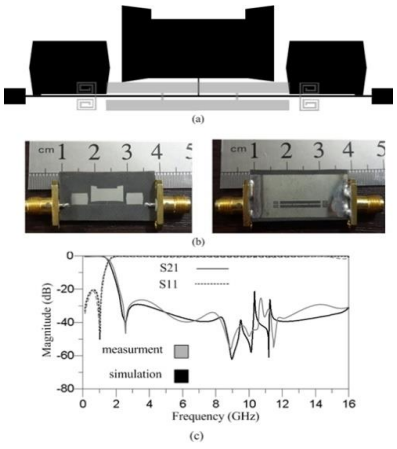

Fig. 7. Proposed LPF: (a) layout, (b) fabrication picture, and (c) simulation and measurement results.

IV. RESULTS DISCUSSION

The LPF has a sharpness of 0.58 GHz with the rate of 29.3 dB/GHz and a cutoff frequency at 1.53 GHz. According to the measurement results, the stopband of this filter is expanded from 2.11 GHz to 16 GHz with more than 24 dB attenuation level. Table 1 compares the performance of the proposed filters with the referenced works. This comparison is based on the equations that are shown in Table 2. These equations describe the sharpness, stopband rejection level, stopband bandwidth, physical size and architecture of the proposed filter and referenced work. The α_{max}, α_{min}, f_s, f_c and λ_g are introduced in the Table 3.

Table 1: Performance comparison among proposed filters and referenced works

Ref.	fc	RSB	SF	ς	NCS	AF	FOM
This work	1.53	9.1	2.4	29.3	0.0075	2	42660
[4]	2.49	1.69	2	54.8	0.0323	1	5734
[5]	2.28	5.47	2	121.4	0.0338	1	39293
[6]	2.3	1.56	2.7	188.9	0.207	2	796
[7]	1.76	7	2	51.5	0.048	1	15021
[8]	2.2	12.8	2	58.6	0.055	1	27276
[9]	2	5.15	2	24.29	0.0094	1	26627
[10]	1.8	2.8	1.6	34	0.031	1	4914
[11]	1.8	16.5	2	250	0.251	2	16434
[12]	2.07	8.62	2.4	36.17	0.0621	1	12050
[13]	2	11.2	1	21.25	0.0078	1	30649
[14]	5.3	0.85	3.5	160	0.391	2	609
[15]	2.2	2.4	2.3	85	0.051	2	4600
[16]	1.3	9.4	1.7	21	0.0088	1	38134
[17]	3.09	4.91	2	45.95	0.031	1	14555

Table 2: Filter specifications and its equations

Equation	Specifications
$\zeta = \frac{a\max - a\min}{fs - fc}$	Sharpness in dB/GHz
$SF = \frac{\text{max attenuation level in stopband}}{10}$	Suppression factor
$RSB = \frac{\text{stopband bandwidth}}{fc}$	Relative stopband bandwidth
$NCS = \frac{\text{physical size}}{\lambda g^2}$	Normalized circuit size
AF	Architecture factor, which is signed as 1 when the design is 2D and as 2 when the design is 3D
$FOM = \frac{\xi \times \text{RSB} \times \text{SF}}{NCS \times AF}$	Figure-of-merit (FOM) is the overall index of the filter

Table 3: Description of the αmax, αmin, fs, fc and λg

Phrase	Description
α_{max}	3 dB attenuation point
α_{min}	20 dB attenuation point
fs	20 dB stopband frequency
fc	3 dB cutoff frequency
λ_g	Guided wavelength at cutoff frequency

As it is shown in Table 1 the FOM of the proposed filter is greater than those of [4-17].

V. CONCLUSION

A high performance lowpass filter, based on the taper loaded resonator is designed, fabricated and measured. The physical size of this filter is 0.15 λg × 0.05 λg and as indicated in the results, the cut off frequency is 1.53 GHz, the roll-off rate is better than 29.3 dB/GHz, the insertion loss is less than 0.1 dB from DC to 1.1 GHz and the rejection is greater than 24 dB from 2.11 to 16 GHz.

ACKNOWLEDGMENT

Author would like to thank Dr. Behzad Ghanbari for his technical support.

REFERENCES

[1] A. S. Al-Zayed, M. B. Asad Allah, and S. F. Mahmoud, "Lowpass filter design based on microstrip meander line with HDGS," *The Applied Computational Electromagnetics Society*, vol. 29, no. 6, 2014.

[2] G. Zhang, J. Wang, Y. Dou, and H. Cui, "Compact microstrip lowpass filter with ultra-wide stopband using stepped-impedance tyrapezoid resonators," *The Applied Computational Electromagnetics Society*, vol. 29, no. 4, 2014.

[3] Y. Dou, J. Wang, H. Cui, and J. L. Li, "Miniaturized microstrip lowpass filter with ultra-wide stopband," *The Applied Computational Electromagnetics Society*, vol. 28, no. 7, 2013.

[4] R.-Y. Yang, Y.-L. Lin, C.-Y. Hung, and C.-C. Lin, "Design of a compact and sharp rejection low-pass filter with a wide stopband," *Journal of Electromagnetic Waves and Applications*, vol. 26 pp. 2284-2290, 2012.

[5] S-V. Makki, A. Ahmadi, S. Majidifar, H. Sariri, and Z. Rahmani, "Sharp response microstrip LPF using folded stepped impedance open stubs," *Radioengineering Journal*, vol. 22, pp. 328-332, 2013.

[6] J. Chen, Z.-B. Weng, Y.-C. Jiao, and F.-S. Zhang, "Lowpass filter design of Hilbert curve ring defected ground structure," *Progress In Electromagnetics Research PIER*, vol. 70, pp. 269-280, 2007.

[7] H. Cao, W. Ying, H. Li, and S. Yang, "Compact lowpass filter with wide stopband using novel windmill resonator," *Journal of Electromagnetic Waves and Applications*, vol. 26, pp. 2234-2241, 2012.

[8] H. L. Cao, W. B. Ying, H. Li, and S. Z. Yang, "Compact lowpass filter with ultra-wide stopband rejection using meandered-slot dumbbell resonator," *Journal of Electromagnetic Waves and Applications*, vol. 26, pp. 2203-2210, 2012.

[9] M. H. Yang, J. Xu, Q. Zhao, L. Peng, and G. P. Li, "Compact, broad-stopband lowpass filters using SIRs-loaded circular hairpin resonator," *Progress In Electromagnetics Research PIER*, vol. 102, pp. 95-106, 2010.

[10] Q. He and C. Liu, "A novel low-pass filter with an embedded band-stop structure for improved stop-band characteristics," *IEEE Microwave and Wireless Components Letters*, vol. 19, pp. 629-631, 2009.

[11] H. Taher, "Ultrawide stopband low-pass filter using triangular resonators defected ground," *Journal of Electromagnetic Waves and Applications*, vol. 28, pp. 542-550, 2014.

[12] M. Hayati, S. Majidifar, and O. S. Fathabadi, "Compact microstrip lowpass filter with wide stopband and high attenuation," *Microwave Journal*, vol. 4, Apr. 2012.

[13] M. H. Yang, J. Xu, Q. Zhao, and X. Sun, "Wide-stopband and miniarurized lowpass filters using SIRs-loaded hairpin resonators," *Electromagnetic Waves and Applications*, vol. 28, pp. 542-550, 2014.

[14] L. H. Weng, S. J. Shi, X. Q. Chen, Y. C. Guo, and X. W. Shi, "A novel CSRRs DGS as lowpass filter," *Journal of Electromagnetic Waves and Applications*, vol. 22, pp. 1899-1906, 2008.

[15] S-H. Fu, C-M. Tong, X-M. Li, W. Zhang, and K. Shen, "Compact miniaturized stepped impedance low-pass filter with sharp cut off characteristic," *Microwave and Optical Technology Letters*, vol. 51, pp. 2257-2258, 2009.

[16] L. Ge, J. P. Wang, and Y.-X. Gue, "Compact microstrip low-pass filter with ultra-wide stopband," *Electronics Letters*, vol. 46, pp. 689-691, 2009.

[17] H. Sariri, Z. Rahmani, A. Lalbakhsh, and S. Majidifar, "Compact LPF using T-shaped resonator," *Frequenz Journal*, vol. 67, pp. 17-20, 2013

[18] W. Che, Y. F Tang, J. Zhang, and Y. L. Chow, "Formulas of dielectric and total attenuations of a microstrip line," *Radio Science*, vol. 45, 2010.

[19] J. S Hong and M. J. Lancaster, *Microstrip Filters for RF/Microwave Applications*, John Wiley & Sons, 2001.

Sohrab Majidifar received his B.Sc. and M.Sc. in Electrical Engineering from Razi University of Kermanshah in 2009 and 2011 respectively. He joined Kermanshah University of Technology in 2011 as a Lecturer. He has published more than 18 papers in international journals and conferences. His research interests include microwave passive circuits, microwave sensors, chipless RFID and RFIC.